Journal of Colloid and Interface Science 608 (2022) 1094–1104

Contents lists available at ScienceDirect

Journal of Colloid and Interface Science

journal homepage: www.elsevier.com/locate/jcis

Effects of particle size on the electrocoalescence dynamics and arrested morphology of liquid marbles

Yage Zhang [a,1], Chentianyi Yang [a,1], Shuai Yuan [a], Xiaoxue Yao [b], Youchuang Chao [a], Yang Cao [a], Qingchun Song [a], Alban Sauret [c], Bernard P. Binks [d], Ho Cheung Shum [a,*]

[a] Department of Mechanical Engineering, University of Hong Kong, Pokfulam Road, Hong Kong, China
[b] Department of Biomedical Engineering, Shenzhen University, Shenzhen 518000, China
[c] Department of Mechanical Engineering, University of California, Santa Barbara, CA 93106, USA
[d] Department of Chemistry, University of Hull, Hull HU6 7RX, UK

GRAPHICAL ABSTRACT

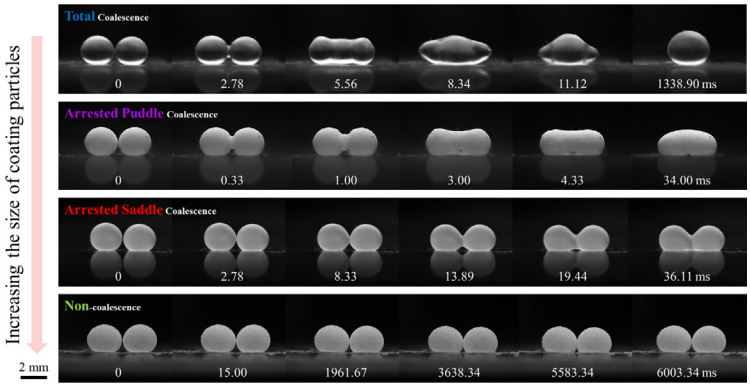

ARTICLE INFO

Article history:
Received 22 April 2021
Revised 28 September 2021
Accepted 28 September 2021
Available online 12 October 2021

Keywords:
Liquid marble
Coalescence
Arrested structure

ABSTRACT

Hypothesis: The coalescence of bare droplets when surface tension dominates always results in one larger spherical droplet. In contrast, droplets coated with particles may be stabilized into non-spherical structures after arrested coalescence, which can be achieved by different approaches, such as changing the particle surface coverage. The size of particles coating the initial liquid marbles can be used to control the coalescence dynamics and the resulting morphology of arrested droplets.
Experiment: We characterized the electrocoalescence of liquid marbles coated with particles ranging from hundred nanometers to hundred micrometers. The electrocoalescence was recorded using high-speed imaging.
Findings: When the electrocoalescence initiates, particles jam and halt the relaxation of the marbles at different stages, resulting in four possible final morphologies that are characterized using the Gaussian curvature at the neck region. The four regimes are total coalescence, arrested puddle coalescence, arrested saddle coalescence, and non-coalescence. The coalescence is initiated at the center of the contact

* Corresponding author at: 7-25, Haking Wong Building, University of Hong Kong, Pokfulam Road, Hong Kong, China.

E-mail addresses: zhangyage@connect.hku.hk (Y. Zhang), ycty@connect.hku.hk (C. Yang), ysthoth@connect.hku.hk (S. Yuan), 2172243110@email.szu.edu.cn (X. Yao), ychao@connect.hku.hk (Y. Chao), yangcao1@connect.hku.hk (Y. Cao), u3006506@hku.hk (Q. Song), asauret@ucsb.edu (A. Sauret), B.P.Binks@hull.ac.uk (B.P. Binks), ashum@hku.hk (H.C. Shum).

[1] These authors contributed equally to this work.

https://doi.org/10.1016/j.jcis.2021.09.187

zone, independent of the particle size. Small particles show little resistance to the coalescence, while marbles coated by large particles demonstrate a viscous-like behavior, indicated by the growth of the liquid bridge and the damping. The present study provides guidelines for applications that involve the formulation of liquid marbles with complex morphologies.

1. Introduction

Coalescence is the process by which two or more sub-entities merge after contact to form one larger entity [1]. The length scale of this process covers a wide range, from the coalescence of micro- and milli-sized droplets and bubbles [2] to the formation of kilometer-sized planets and stars [3,4]. The coalescence dynamics of droplets is involved in many industrial applications, such as inkjet printing and foam stability [5,6]. The initiation of the coalescence between two liquid droplets put in contact at a negligible relative velocity first occurs through the formation of a liquid bridge. The coalesced droplet then oscillates before stabilizing into a larger spherical shape. Different physical quantities, such as the viscosity, can affect the intermediate behavior of the coalescence [7,8]. Nevertheless, in systems dominated by surface tension other than elastic force, coalesced droplets always stabilize into a spherical equilibrium state [9]. However, non-spherical systems, from cellular organelles [10] to bubbles in whipped cream, abound in daily lives. Many of these anisotropic microstructures are derived from the coalescence of smaller constituents. The ability to coalesce and stabilize liquids with a prescribed shape leads to new insights into pharmaceutical formulations and food processes [11–13]. However, the coalescence of bare non-viscoelastic droplets can hardly achieve this goal, and methods to control the shape of droplets obtained from coalescence remain poorly explored.

A method to generate non-spherical droplets relies on the interfacial jamming of particles that stabilize the droplets [14,15]. Particles at interfaces have been studied for their ability to stabilize non-equilibrium fluid structures, for instance, during the fusion of bubbles [16,17] and the preparation of bicontinuous interfacially jammed emulsion gels ('bijels') [18,19]. The stabilization can be achieved using different approaches. In the Pickering emulsions system [20], non-spherical emulsion droplets can be obtained by manipulating the surface coverage of particles [21,22]. Liquid-liquid interfaces coated with micron-sized particles [23,24] and non-spherical armored bubbles [25,26] have been widely studied. However, the effects of the particle size on the coalescence dynamics and the resulting final shape of armored droplets remain elusive.

To address this question, we consider liquid marbles, which are liquid droplets stabilized by hydrophobic particles in a gaseous environment. Liquid marbles are a convenient system to study as they are easy to prepare [27,28]. A DC electric field is applied to drive the coalescence until the resulting marble stabilizes to a final shape. Once the coalescence is initiated, the larger the size of the coating particles, the earlier the coalescence is arrested. The degree of arrest is quantified by the Gaussian curvature at the neck bridging the two liquid marbles. The final morphology is categorized into four distinct regimes: (i) total coalescence, (ii) arrested puddle coalescence, (iii) arrested saddle coalescence, and (iv) non-coalescence, respectively. The coalescence dynamics of liquid marbles coated with particles of different sizes is recorded using high-speed imaging. The coalescence is initiated at a single patch close to the center of the contact region, regardless of the size of the stabilizing particles. However, the coalescence dynamics then depends on the particle size. The differences can be observed during the growth of the liquid bridge at short-timescale (∼2 ms) and during the subsequent long-timescale oscillations of the liquid marble (∼20–200 ms). To the best of our knowledge, this is the first time that the growth of the liquid bridge between armored droplets is measured and quantified. In the regimes of total coalescence and arrested puddle coalescence, the growth of the liquid bridge follows a square root relation with time, similar to what is observed for bare liquid droplets [29]. The growth of the liquid bridge in the arrested saddle regime shifts from a square root to a linear evolution with time. Such a linear scaling law is also observed for the coalescence of bare droplets with large viscosity where the viscous force is dominant [7]. The subsequent oscillations in the arrested coalescence regimes experience a critical damping, different from the under-damping observed in the total coalescence regime. Different damping models based on the damping ratios are considered to rationalize our observations. The growth of the liquid bridges and the damped oscillations demonstrate that the arrested coalescence can stabilize at a faster rate. The heavily damped behavior of liquid marbles during arrested coalescence also exhibits a viscous-like behavior. The present investigation offers new insight for applications involving liquid marbles and other stabilized emulsion droplets by providing guidelines to coalesce and arrest liquids with a prescribed shape.

2. Materials and methods

2.1. Materials

In previous studies, particles made up of a wide variety of materials and shapes have been used to prepare the liquid marbles. Common materials include silica [27], lycopodium [27], polytetrafluoroethylene (PTFE) [30], and silicone resins [31]. The liquid marbles can be formed using particles of different shapes, including cubes [32], plates [33], and sheets [34]. In the present study, liquid marbles have been prepared using particles and powders of different materials, sizes, and shapes. The wettability, composition, and morphology of the particles were expected to affect their interfacial behavior. For instance, for liquid marbles formed using the electrostatic method, an increase in the conductivity of particles permits lower particle size transfer and successful liquid marble preparation [35]. Nevertheless, we used the regular rolling method rather than electrostatic methods to prepare liquid marbles so that differences in electrical properties of the particles would not affect the preparation of the liquid marbles. Moreover, we selected particles with properties as similar as possible so that the large difference in size between the particles would be the main parameter changed between experiments. The nanoparticles used in this study included fumed silica nanoparticles treated with dichlorodimethylsilane (DCDMS) (Aerosil R972 and R974, with primary particle size 16 and 12 nm, and particle-water contact angle of 117° and 105°, respectively, Evonik, Germany) and with hexamethyldisilazane (HMDS) (Aerosil R812, primary diameter of 7 nm, particle-water contact angle of 118°, Evonik, Germany). Silicone resin particles of diameter 2.0 μm, 4.5 μm, and 6.0 μm were purchased from Momentive Performance Material Inc., Japan, all with a particle-water contact angle of 91°. Other particles also included silicone particles (diameter of 3.5 μm, 5.0 μm, 12 μm, and 20 μm, all

with a contact angle of 120°, NanoMicro Tech. Inc., China), silica particles (diameter of 10 μm, Nanjing Gen-Shine Tech. Inc., China), and polystyrene particles (diameter of 50 μm and 100 μm, contact angle of 95°, NanoMicro Tech. Inc., China). Powders used in this project included 1 μm polytetrafluoroethylene (PTFE) grains (particle-water contact angle of 110°, Sigma-Aldrich, USA), lycopodium powder (diameter of 35 μm, Sigma-Aldrich, USA) and fluorinated graphene nanoplates (lateral size of 0.2–3 μm, thickness of 3–10 nm, Ashine Tech. Inc., China). SEM and TEM images of representative particles are shown in Table S1, where most microparticles show spherical shapes, while nanosized particles are non-spherical. A zetasizer (Malvern Pro) was applied to measure the equivalent size of nanoparticles. The average size for fumed silica nanoparticles (R812) and graphene nanoplates are 0.27 μm ± 0.0 1 μm and 1.36 μm ± 0.13 μm, respectively (Fig. S1). Deionized (DI) water was collected from Direct-Q (Merck Millipore) and was used as the liquid phase for all the experiments unless otherwise noted. For experiments where a viscous liquid phase was used, glycerol purchased from Sigma-Aldrich (≥99.5%) was used to increase the viscosity. Poly(dimethylsiloxane) (PDMS) and the curing agent were purchased from Dow Corning, USA. The dielectric layer was prepared by mixing PDMS and curing agent at a weight ratio of 10:1; the mixture was then poured gently on a cleaned glass slide followed by spin coating (WS-650MZ-23NPPB, Laurell). The thickness of the dielectric layer was measured by a profilometer (DektakXT, Bruker).

2.2. Preparation of liquid marbles

The volume of the droplet phase was controlled by a micropipette (Rainin Pipet-Lite XLS, 2–20 μL). Liquid marbles were prepared by first dispensing the targeted volume of liquid onto a plastic cell culture dish (LabServ, 35 mm × 12 mm) covered with particles. Then the dish was gently vibrated to allow particles to cover entirely the air–liquid interface. After that, two plastic spoons were used to gently move the liquid marbles from the particle bed to the experimental setup. During the process, spoons were also gently twisted manually to allow the liquid marble to move back and forth, removing excess particles assembled at the liquid–air interface.

2.3. Experimental setup

Two custom-made experimental setups were used in this project. The main setup consisted of a lifting platform, a light-emitting diode (LED) light source, a high-voltage supply (Tianjin Dongwen, China), a high-speed camera (Photron Fastcam SA3) equipped with a Nikon AF Micro 60MM F/2.8D lens, a digital camera, a printed circuit board (PCB) with embedded electrodes and a computer for monitoring. The PCB was fixed on the lifting platform, with the high-voltage supply connected to two adjacent embedded electrodes on the PCB. A dielectric PDMS layer was placed on top of the electrodes, and the LED light source was fixed on the lifting platform. The high-speed camera and the digital camera were used to record the lateral side view and top view of the coalescence process, respectively. A schematic of the experimental setup is shown in Fig. 1a. All images and videos recorded were processed using ImageJ (National Institutes of Health, USA). Another customized setup was used to visualize the dynamics at the contact region of one liquid marble when the coalescence is initiated (see schematic in Fig. S2). Similar to the setup above, the PCB board was fixed on the lifting platform but only one embedded electrode was soldered and connected to the ground of the high-voltage supply. An indium tin oxide (ITO) glass slide was glued and fixed next to the electrode, perpendicularly to the PCB board, and connected to the positive pole of the voltage supply. The high-speed camera was placed next to the lifting platform, focusing on the conductive surface of the ITO glass where the liquid marble would make contact. The dynamics at the contact region of the marble with the ITO glass was then recorded and later processed using ImageJ.

2.4. Electrostatics-driven coalescence of liquid marbles

After preparation, two liquid marbles were moved onto the electrodes leaving a narrow gap between them before applying the voltage. The narrow gap was much smaller than the size of the marbles, as shown in the supplementary videos, and did not influence the final arrested shape. The voltage was applied to the two embedded electrodes by connecting the high DC voltage supply to two metal wires soldered at the back of the PCB and was gradually increased manually. The electrostatic force moved the marbles in contact with each other, and a sufficient voltage applied to the electrodes triggered the coalescence [31]. The side-view morphology was sampled at 3600 frames per second (fps) unless stated otherwise, and the top-view was recorded by the digital camera at 60 fps. All experiments were conducted at room temperature of 20 °C and relative humidity of 50%.

2.5. Characteristics of interfacial properties of liquid marbles

The interfacial properties of the liquid marbles were measured experimentally. The effective surface tensions of liquid marbles coated with particles of different sizes were obtained using the puddle height method [36]. The corresponding effective surface tensions were comparable, with values varying between 59.4 and 66.9 mN/m (Fig. S3). In addition, the number density of liquid marbles, which was defined as the number of particles per unit area, was measured experimentally and estimated theoretically [37] (Table S2). The predicted number density decreases from 1.59×10^7 mm^{-2} to 4.63×10^2 mm^{-2} with the increment of particle size from 0.27 μm to 50 μm. Experimental data showed that liquid marbles stabilized by smaller particles had larger particle densities, which agreed in tendency with the number density predicted by models.

3. Results and discussion

3.1. Arrested coalescence of liquid marble triggered by electrostatics

The coalescence of two liquid droplets placed on a superhydrophobic substrate results in a spherical droplet of larger volume since the surface tension minimizes the interfacial energy of the system [38]. However, when particle stabilizers are introduced so that the droplets form liquid marbles, the surface-tension-dominated coalescence can result in arrested structures.

The stability of liquid marbles strongly depends on the compact particle layer at the air/liquid interface resulting from the particle interactions. The size of the particles used in this study varies from hundreds of nanometers (average size 270 nm) to hundreds of micrometers (~100 μm). Therefore, the interactions among the different particles differ. The van der Waals force is a short-range attraction [39,40] and dominates the interaction between nanoparticles to form larger aggregates (Fig. 1b and c). The microparticles exhibit a compact arrangement but do not form aggregates, as shown in Fig. 1c and d. In all cases, stable liquid marbles have a high particle coverage Γ. The theoretical surface coverage of a monolayer of particles packed in a hexagonal lattice is $\Gamma \approx \pi/\left(2\sqrt{3}\right) \approx 0.907$ [41]. Experimentally, the surface coverage Γ typically reaches 0.8 to 0.9 [42,43]. Therefore, particles have limited space to re-distribute on the interface regardless of their size, as shown in Fig. 1b–e. Once the coalescence is initiated, the parti-

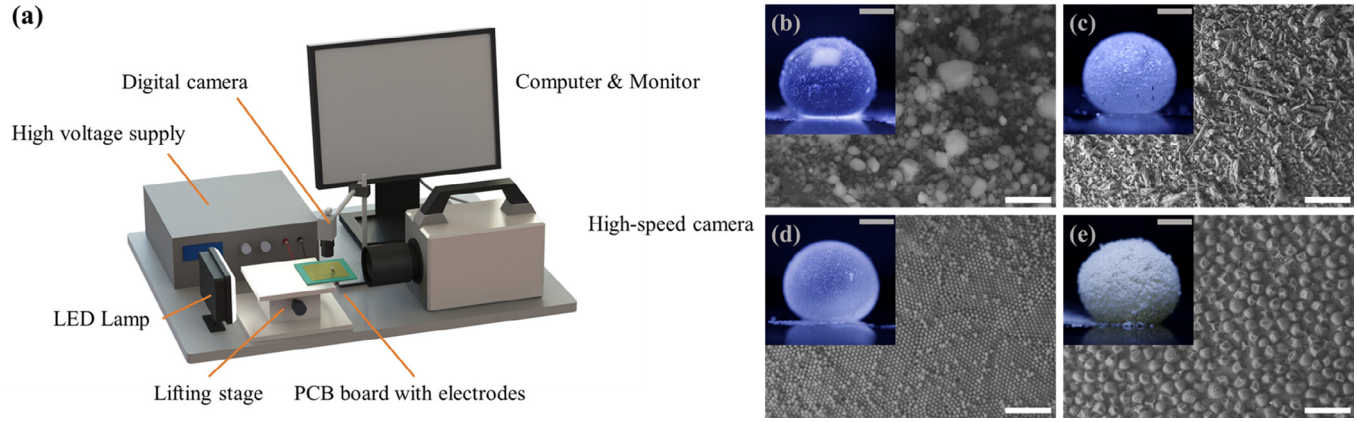

Fig. 1. (a) Experimental setup for the arrested electrocoalescence of liquid marbles. (b)–(e) 10 μL of 40% aqueous glycerol liquid marbles (inset) and corresponding SEM images of the liquid–air interface using (b) fumed silica nanoparticles of primary diameter 7 nm, (c) graphene nanoplates of size 0.5–5 μm, (d) 10 μm silica particles, and (e) 35 μm lycopodium granules. Aqueous glycerol is chosen since its high viscosity impedes an easy rupture of the liquid marbles on the rough SEM cold stage. Scale bars represent 1 mm in insets and represent 100 μm in the SEM micrographs.

cles may either detach from the liquid–air interface without impeding the coalescence process or jam at the interface leading to a loss of interfacial mobility. The detachment energy of a spherical particle from a gas–water interface to the gas phase can be estimated as $E = \pi R_{particle}^2 \sigma_{air-liquid}(1+\cos\theta)^2$, where $R_{particle}$ is the radius of the particles covering the liquid marble, $\sigma_{air-liquid}$ is the surface tension, and θ is the contact angle between the particle and the liquid [44]. We used in this study hydrophobic particles with contact angles ranging from 91° to ~120°, and their sizes vary from hundreds of nanometers to ~100 μm. In the expression of the detachment energy, for a given size of particle, the term containing the contact angle $(1+\cos\theta)^2$ would incur at most a 4 times difference in our experiments. The variation induced by tuning the particle size is several orders of magnitude larger than the variation due to a change of the contact angle for the range of parameters considered in this study. Therefore, the size of the coating particles is a more critical parameter determining whether they remain at the air–liquid interface or not after coalescence.

In our experiments, the coalescence of liquid marbles is triggered electrostatically. A dielectric layer separates the liquid marbles and the charging electrode; hence the applied voltage does not significantly affect the interfacial properties of the stabilizing particles. A sufficiently large voltage exerts an electrostatic force *via* the induced charges on the interface of the two marbles and draws liquid tips, which then contact and form a liquid bridge [31]. The liquid bridge keeps expanding while the particles at the air/liquid interface impede the process by jamming at the connecting neck region between the two marbles. The shape of the resulting marble obtained after coalescence depends markedly on the size of the particles that encapsulate the droplet phase for a given liquid. Different coalescence dynamics of liquid marbles are observed when the size of the coating particles increases from hundreds of nanometers to hundreds of micrometers, as illustrated in Fig. 2. For nanoparticles, the electrocoalescence of two liquid marbles leads to a final spherical shape, illustrated in Fig. 2a; we refer to this as total coalescence. When the size of the stabilizing particles increases, the electrocoalescence can still be initiated, but the resulting shape is not fully spherical and is called arrested. Liquid marbles coated with nanoplates lead to such an arrested coalescence, as shown in Fig. 2b. The resulting marble maintains a puddle shape from the side view, while the curvature of the neck region where the coalescence initiates becomes much lower. Another type of arrested coalescence is usually observed when the size of the stabilizing particles increases to several micrometers (in this example, 6 μm). The resulting curvature of the upper part is negative and the marble exhibits a saddle shape, as illustrated in Fig. 2c. The PCB boards with embedded electrodes can only withstand a limited voltage before a breakdown so that we manually set a maximum applied voltage at 1 kV. As the particle size reaches 35 μm, the threshold voltage drives them in contact but remains insufficient to trigger the electrocoalescence of the two liquid marbles. This is referred to as the non-coalescence regime, as illustrated in Fig. 2d. It should be noted that marbles are flattened during the process, which is attributed to the electro-wetting behavior under high electric potential [45]. More sizes and types of particles have also been tested on liquid marbles of volume 10 μL, and their resulting shapes are reported in the Supplementary Information (Table S3). These results demonstrate that the particle size is a critical parameter that governs the morphology of the resulting marble after coalescence. The static and dynamic profiles of the coalescence behavior will be discussed in the following sections.

3.2. Regimes of coalescence defined by Gaussian curvature

The final morphology of the coalesced marble reflects the static outcome of the coalescence behavior resulting from the jamming of the particles. We consider the Gaussian curvature at the neck connecting the two liquid marbles to characterize the influence of the size of the jammed particles on the morphology of the arrested marble [46]. The Gaussian curvature K is given as:

$$K = \kappa_1 \kappa_2 \tag{1}$$

where κ_1 and κ_2 are the two principal curvatures at the top center point of the neck region where the coalescence of the two liquid marbles LM_1 and LM_2 is initiated (see schematic in Fig. 3a). Without loss of generality, κ_1 is defined as the curvature in the *y*-*z* plane and κ_2 is the curvature in the *x*-*y* plane. The detailed calculation of the Gaussian curvature with illustrative Figs. S4 and S5 are given in the Supplementary Information. For a spherical 20 μL liquid marble resulting from the coalescence of two 10 μL ones and neglecting gravitational effects, κ_1 and κ_2 are equal. The normalized Gaussian curvature is expected to be K = 2.29. The details of the normalization can be found in the Supplementary Information. In our experiment, we choose a 20 μL bare water droplet as a benchmark for the total coalescence. We determine its Gaussian curvature K = 1.96, with κ_1 and κ_2 being 1.36 and 1.44, respectively. The confidence range can thus be obtained as $K = 1.96 \pm 0.11$ for the total coalescence case in view of the assumed isotropic symmetry. A difference

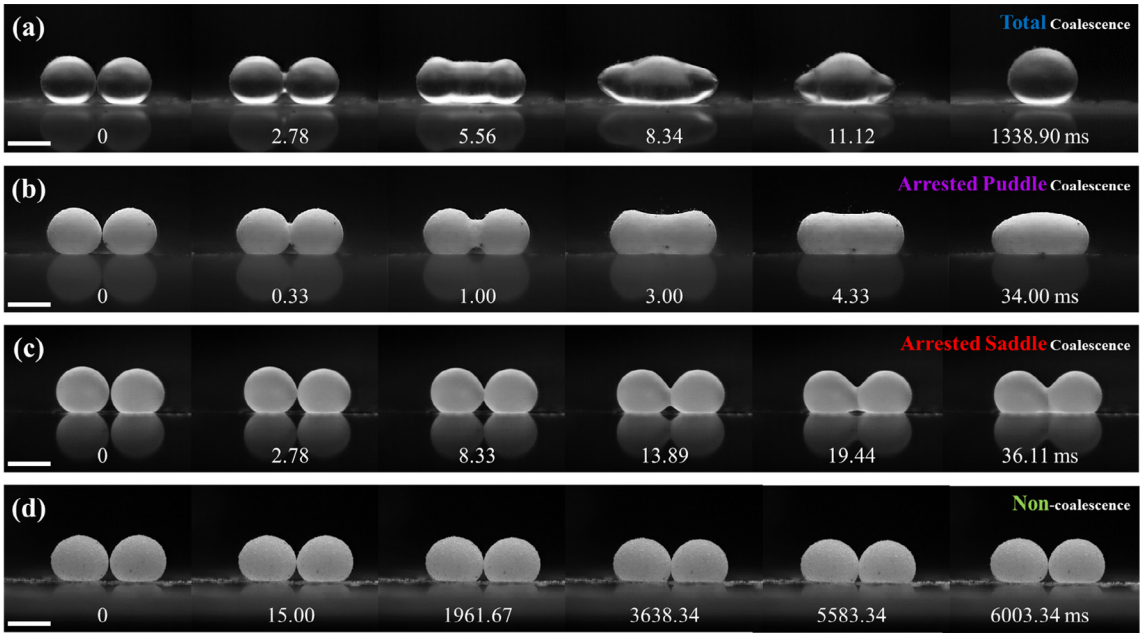

Fig. 2. Representative images of electrocoalescence of liquid marbles coated with different particles. (a) Total coalescence regime from liquid marbles coated with R812 silica nanoparticles (primary diameter 7 nm). Arrested coalescence regime with either (b) a puddle shape from liquid marbles coated with graphene nanoplates (lateral size 0.2–5 μm) or (c) a saddle shape from liquid marbles coated with 6 μm silicone resin particles. (d) Non-coalescence for liquid marbles coated with 35 μm lycopodium particles. Scale bars are 2 mm.

between κ_1 and κ_2 is expected for arrested coalescence (Fig. 3c and d). If droplets are covered with large particles (≥35 μm here), the coalescence cannot be initiated, and the corresponding Gaussian curvature is by definition negative infinity (Fig. 3e). We can quantitatively separate the different arrested morphologies into four different regimes as a function of the Gaussian curvature, namely total coalescence ($2.07 > K > 1.85$), arrested puddle coalescence ($1.85 > K > 0$), arrested saddle coalescence (K finite and negative) and non-coalescence ($K = -\infty$).

The values of the Gaussian curvature for the different arrested morphologies obtained by the electrocoalescence of two marbles are shown in Fig. 3f. The curvature generally decreases when increasing the size of the coating particles. However, we notice that the absolute value of the Gaussian curvature of marbles coated with 10 μm silica particles is smaller than that of those coated with 6 μm silicone resin particles. This observation is likely due to an electro-wetting phenomenon under high voltage [45]. As the size of coating particles increases, the voltage triggering the coalescence also increases (as reported in Table S4), which leads to a change of contact angle between the lower surface of the marble and the substrate. As a result, the wetting effect becomes more prominent when 10 μm particles are used, and the resulting marble flattens at the region where the Gaussian curvature is defined. Therefore, the marbles coated with 10 μm silica particles show a curvature with an absolute value smaller than those with 6 μm particles.

The behavior associated to the electrocoalescence of two liquid marbles (LM_1 and LM_2, respectively) coated by particles of different sizes is systematically investigated by varying the size of the particles d_1 and d_2 on the two marbles. The mapping of the four distinct coalescence regimes as a function of the size of the stabilizing particles is reported in Fig. 3g, based on the Gaussian curvature calculated as above. Since d_1 and d_2 are interchangeable, the data presented in Fig. 3g are symmetrical.

The arrested stabilized liquid marbles have a finite internal stress due to the Laplace pressure imbalance:

$$\Delta P = \sigma_{air-liquid}\left[\frac{2}{R_{marble}} - \left(\frac{1}{\kappa_1} - \frac{1}{\kappa_2}\right)\right] \quad (2)$$

where $\sigma_{air-liquid}$ is the liquid-air surface tension, κ_1 and κ_2 are the two principal curvatures, and $1/R_{marble}$ is the curvature at the leftmost or rightmost point on the marble. Water is used as the droplet phase for all coalescence experiments to avoid jamming on the marble shell due to the variation in the surface tension of the core liquid [47]. For liquid marbles coated with graphene nanoplates and 6 μm silicone resin particles, the Laplace pressure imbalance is found to be $\Delta P = 79$ Pa and $\Delta P = 129$ Pa, respectively. Such imbalanced stress must be overcome by the elasticity of the jammed interface. No noticeable particle jamming is observed for the total coalescence and arrested puddle coalescence (Fig. 4b and c), while close-packed particles can be observed in the arrested saddle coalescence, as shown in the inset of Fig. 4d. The lack of visible particles packed in the neck region for the former two coalescence regimes does not deny the existence of particle jamming, but can be attributed to the difficulty to visualize nanometric particles [48]. The static internal stress is overcome by the modulus of the compact particle layer, which is expected to be of order $E\,\sigma/R_{particle}$ and thus larger than 10^3 Pa [49]. Since the internal pressure difference ΔP is one order of magnitude smaller, this relatively larger value of the Young's modulus ensures a marginal deformation of the coalesced marbles and leads to a stable non-spherical arrested shape.

3.3. Hydrodynamic behavior during the coalescence of liquid marbles

3.3.1. Initiation of the coalescence

The experimental results, as shown for instance in Fig. 2, suggest a correlation between the size of the coating particles, the timescale of the coalescence and the shape of the arrested marble. However, the location where the coalescence is initiated and the dynamics of how the resulting marble becomes arrested by varying the size of the particles remain unclear. To study the arrest process, we record the coalescence dynamics for liquid marbles stabilized

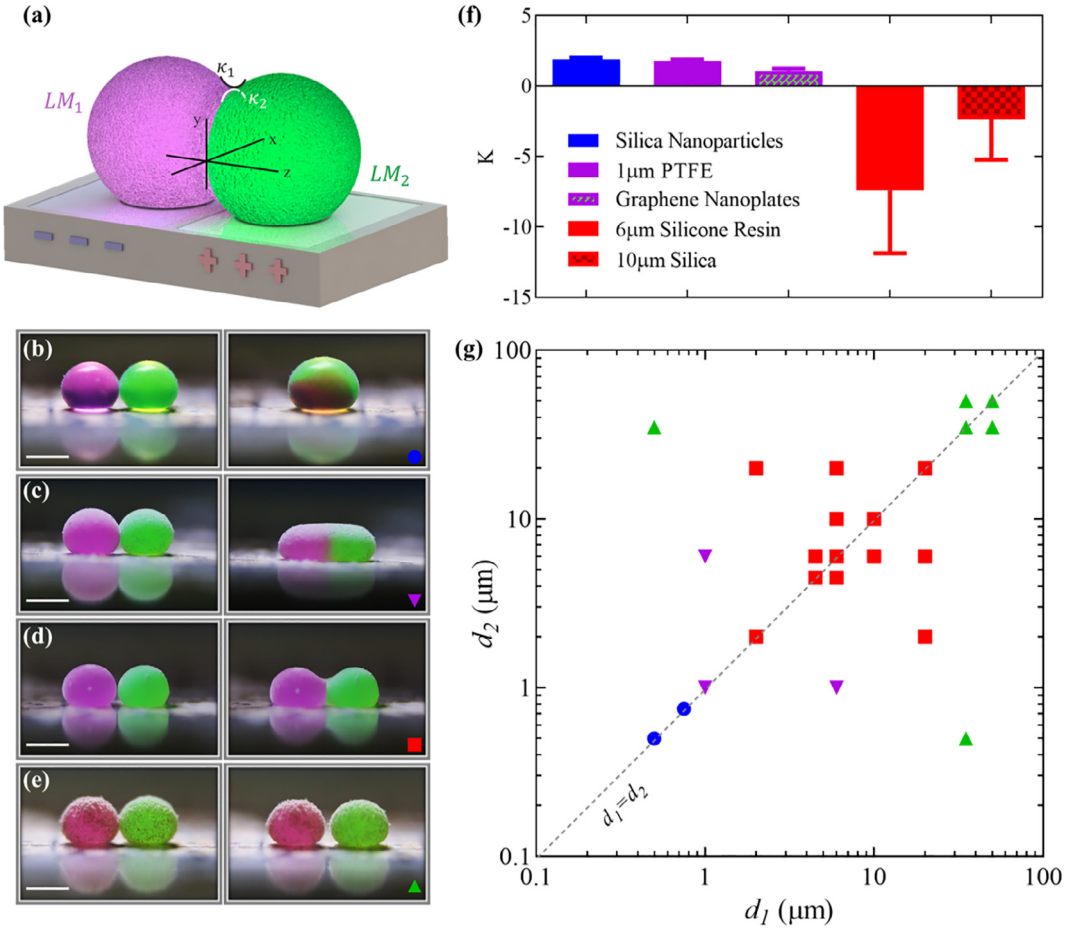

Fig. 3. (a) Schematic of the platform where two liquid marbles are triggered to coalesce by forming a liquid bridge between them. The principal curvatures κ_1 and κ_2 are measured to calculate the corresponding Gaussian curvature K. The morphology of the coalesced marble is determined by the size of the coating particles. (b) Fumed silica nanoparticles of primary diameter 7 nm for total coalescence leading to a Gaussian curvature of $K = 1.92$, (c) graphene nanoplates with a lateral size of 0.2–5 μm and a thickness of 3–10 nm for arrested coalescence with $K = 0.79$, (d) 6 μm silicone resin particles for arrested coalescence with $K = -6.85$, (e) 35 μm Lycopodium particles for non-coalescence with Gaussian curvature of $K = -\infty$. Scale bars are 2 mm. (f) The value of the Gaussian curvature is given for representative marble-marble coalescence, where the two marbles are coated with the same type of particle indicated in the legend of the figure. (g) Different coalescence regimes as a function of the size of the coating particles for two liquid marbles coated by different particles of diameters d_1 and d_2, respectively. The symbols (●), (▼), (■), and (▲) represents the resulting marbles after coalescence in the regimes of total coalescence, arrested puddle coalescence, arrested saddle coalescence, and non-coalescence, respectively.

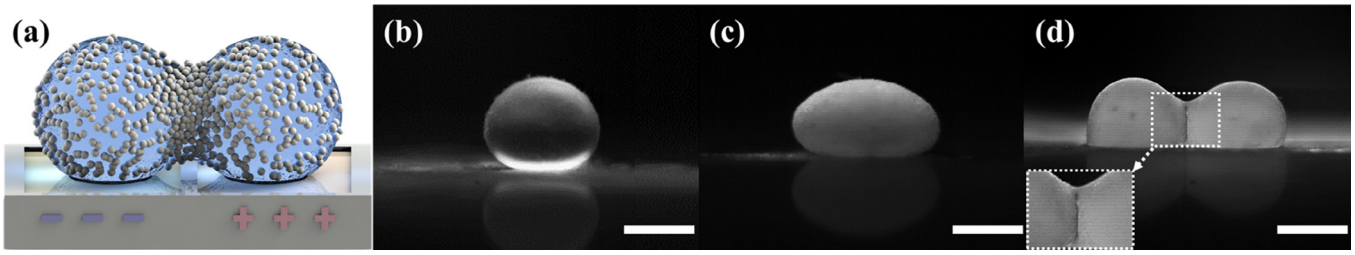

Fig. 4. (a) Sketch of the neck region during the coalescence of liquid marbles. Images of the resulting liquid marble coated with (b) silica nanoparticles, (c) graphene nanoplates and (d) 6 μm silicone resin particles after coalescence. Scale bars are 2 mm.

by particles of different sizes. As the original setup does not allow visualizing the position at which the coalescence is initiated, we built another custom-made setup where a single liquid marble experiences electric stress (Fig. S2). This system is electrostatically equivalent to the original one since the ITO glass is positioned on the surface where the coalescence is initiated and has a constant electric potential. An example of such an experiment is shown in Fig. 5a and Video S1, where the liquid marble coated with graphene nanoplates has a quasi-spherical shape. The high-speed camera focuses on the surface of the ITO glass that makes contact with the marble before the voltage is applied (at time $t = -10$ ms). The rupture of the marble occurs once the applied voltage is sufficient, indicated by the sudden appearance of a region deficient of particles emphasized by the high intensity of the transmitted light. The rupture position is pointed by the white arrow at $t = 0$ ms (Fig. 5a). Once the rupture is initiated, the liquid spills from the marble and wets the ITO slide. By maintaining the voltage, the region without particles increases in size, as shown by the increase in the area of the light zone at two successive times, $t = 10$ ms and $t = 30$ ms.

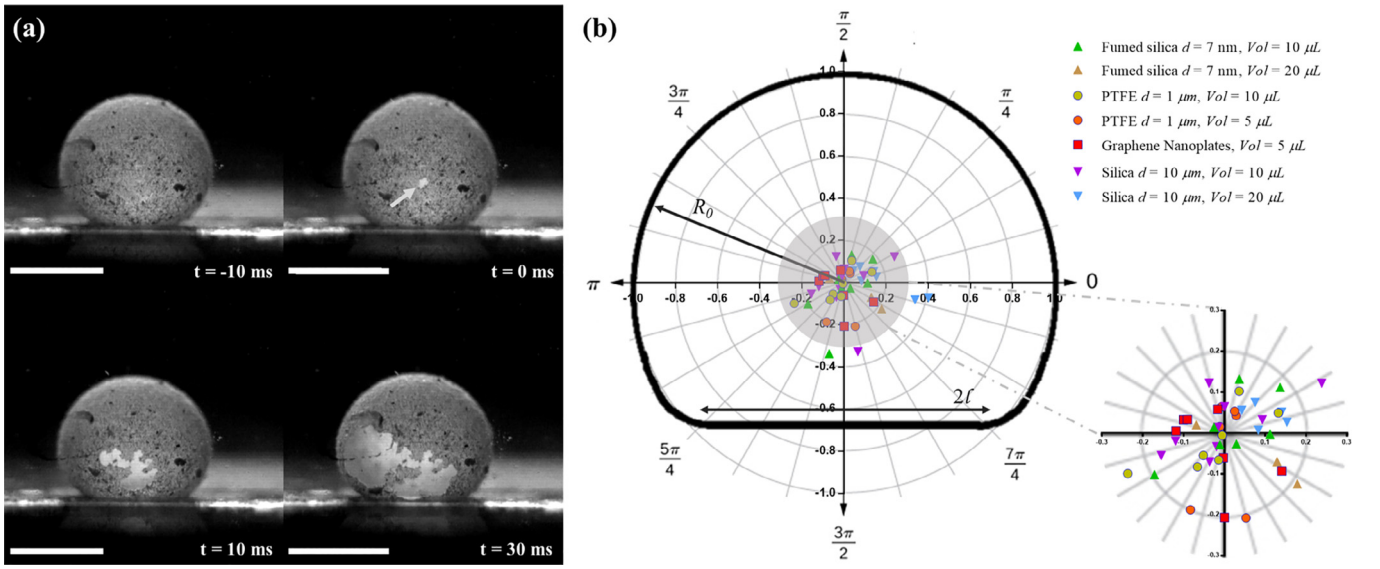

Fig. 5. (a) Series of images showing the interfacial evolution of a typical rupture of a liquid marble coated with graphene nanoplates. Once the rupture is initiated, the encapsulated liquid quickly wets the ITO substrate while particles jam at the boundaries of the rupture position. Maintaining the electrostatic force increases the area of the rupture region and reinforces the jamming of particles. Scale bars are 1.5 mm. (b) Polar plot reporting the locations at which the rupture of electrically charged marbles of different volumes coated with various particles of different size occurs. The length has been normalized by $R^* = R_{pore}/R_{radius}$.

The rupture of a liquid marble under mechanical compression is initiated close to the edge of the contact area [50]. When an electrostatic force is applied, the rupture is instead always initiated around the center part of the contact area as reported in Fig. 5b. We characterize quantitatively the location where the rupture is initiated. The spatial location of the initial rupture is recorded in a polar coordinate system. For each location, the axis is normalized by $R^* = R_{pore}/R_{radius}$, where R_{pore} is the distance between the center of the marble to the pore where the rupture is initiated and R_{radius} denotes the radius of the marble. We systematically characterize the regions where the rupture occurs by testing water marbles of different volumes (5 μL, 10 μL and 20 μL) and with different stabilizing particles (silica nanoparticles, graphene nanoplates, 1 μm PTFE particles, and 10 μm silica particles). In most experiments, the rupture is initiated at locations within the region where R^* ranges from 0 to 0.2, as shown in the polar plot in Fig. 5b. Only in a few cases the coalescence is initiated slightly beyond the [0, 0.2] region. These experiments reveal that the location where the rupture is observed is different between mechanical compression and electrostatics coalescence. Indeed, the direct visualization of the pores at the central spot of the contact zone confirms that the electrocoalescence of liquid marbles is initiated from the conical liquid tips induced by the deformation of the interface of the droplet when a high voltage is applied.

3.3.2. Short-timescale growth of liquid bridge

Although the coalescence is always initiated at a similar location on the liquid marbles, the hydrodynamics process shows significant differences between liquid marbles coated with particles of different sizes, both during the early stage where the liquid bridge forms and during the later stage before the resulting marble is stabilized. Previous studies have reported that the growth of the liquid bridge between two coalescing bare droplets in air (gas–liquid systems) exhibits two distinct behaviors – inertial coalescence and purely viscous coalescence [7,29]. The radius of the liquid bridge, R, follows the scaling law $R \propto \sqrt{t}$ for inertial coalescence and $R \propto t$ for the viscous coalescence. The same scaling has also been observed between droplets in emulsions (liquid–liquid systems) [51]. Here, we tracked the time-evolution of the radius of the liquid bridge of water marbles coated with different particle sizes while using bare water droplets as a control experiment. The liquid bridge of the bare water droplet grows with time as $R \propto t^{\alpha}$, where experimentally $\alpha = 0.501$, as shown by the hexagonal symbols (⬡) in Fig. 6a and Video S1.

A sufficiently large voltage triggers the coalescence once two liquid marbles make contact. Then, the liquid bridge connecting the two marbles can be observed during the early stage of the coalescence process. Two distinct scenarios are observed depending on the system considered: Inertia-dominated coalescence and viscosity-dominated coalescence. In the case of total coalescence (silica nanoparticles) and arrested puddle coalescence (graphene nanoplates and PTFE) of liquid marbles, the time evolution of R is also proportional to $\sqrt{t}$, as shown in Fig. 6a, which is similar to the scaling law observed for the inertial coalescence of bare water droplets. To further illustrate this scaling law, we normalize t and R by the inertial time τ_i and the initial radius R_0, respectively. The inertial time τ_i is defined as $(\rho R_0^3/\sigma)^{1/2}$, where ρ is the density of water and σ is its surface tension. This normalization leads to a scaling law $R/R_0 \propto (t/\tau_i)^{1/2}$ for the bare water droplet (control experiment), and all the marble-marble coalescences mentioned above are shown in the inset of Fig. 6a [7]. All the normalized data are shifted so that the fitting lines go through the origin and all the coalescence processes are set to start at time $t = 0$. The slopes of the fitting lines for the bare water droplets, the liquid marbles coated with silica nanoparticles, 1 μm PTFE particles, and graphene nanoplates are 0.980, 1.028, 0.986 and 1.032, respectively. These experiments show that in the cases of total coalescence (○, Video S2) and arrested puddle coalescence (□, Video S3 and □, Video S4), the coating particles have no observable influence on the initial stage of coalescence that is still described by the scaling law obtained for bare droplets, *i.e.*, $R/R_0 \propto (t/\tau_i)^{1/2}$.

In contrast, for the arrested saddle coalescence, the growth of the liquid bridge when using 6 μm silicone resin-coated marbles (△) is much slower, and a linear behavior better captures the dynamics (Video S5). This behavior is similar to the viscous bare droplet coalescence scenario, where $R \propto t$. We further confirm the inertial-to-viscous transition in the coalescence dynamics of silica nanoparticle-coated marbles by using water-glycerol mix-

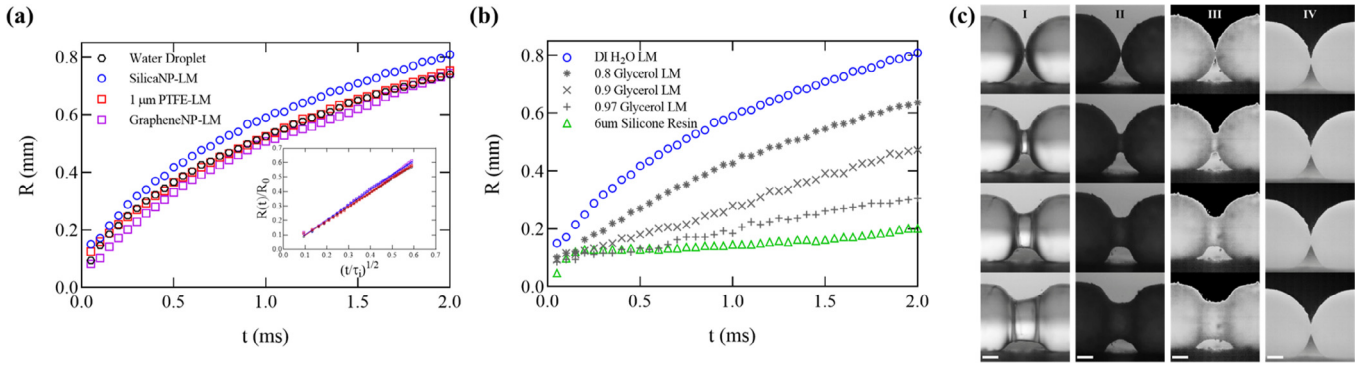

Fig. 6. (a) Time evolution of the radius of the liquid bridge for the case of coalescing bare water droplets (⬡) and liquid marbles coated with either silica nanoparticles (○), 1 μm PTFE particles (□) or graphene nanoplates (□). Inset: collapse of the data when using R_0 and τ_i to re-scale the radius and time. (b) Growth of the liquid bridge of liquid marbles coated by silica nanoparticles in which the encapsulated liquid is water (○), 80 wt% glycerol (✳), 90 wt% glycerol (×), and 97 wt% glycerol (+), respectively. The hydrodynamics of marble-marble coalescence varies from an inertia-dominated regime to a viscous-dominated regime. The arrested saddle coalescence observed with the 6 μm silicone resin particles (△) encapsulating water shows a viscosity-dominated dynamics. (c) Series of images illustrating the initial stage of the coalescence of liquid marbles (from left to right, the coating particles are silica nanoparticles, graphene nanoplates, 1 μm PTFE particles and 6 μm silicone resin particles) taken at 0.05 ms (first frame where the liquid bridge appears), 0.5 ms, 1.0 ms and 1.5 ms, respectively. Scale bars are 0.5 mm.

tures of different viscosities for the droplet phase, as shown in Fig. 6b. The inertia-dominated regime occurs when pure water (○) is encapsulated, while the viscous coalescence regime is observed when the encapsulated droplet is 90 wt% glycerol (×) and 97 wt% glycerol (+), of similar density and surface tension as water but with a much larger viscosity of 160 mPa s and 440 mPa s, respectively. The crossover between the inertia-dominated and viscosity-dominated regimes is observed experimentally at 80 wt% glycerol (✳) corresponding to a viscosity 46.3 mPa s, very close to the value of 50 mPa s reported in a previous study for silicone oil [7]. For water droplets coated with 6 μm silicone resin particles, the growth of the liquid bridge exhibits a linear evolution in time and is even slower than the viscous 97 wt% glycerol marble. Images of the liquid bridge connecting two water marbles coated with particles of various sizes extracted at the same time are shown in Fig. 6c, from time $t = 0.05$ ms to $t = 2$ ms. The radii of the liquid bridges connecting the two liquid marbles increase much faster for total coalescence and arrested puddle coalescence (columns I-III) than for the arrested saddle coalescence (column IV).

3.3.3. Long-timescale oscillation of coalesced marble

The long-time evolution is investigated by characterizing the oscillation of the liquid marble after the initiation of the coalescence. Different damping behaviors are observed depending on the regime of coalescence. The variation in the width of the resulting marble in the lateral direction of coalescence W_x (see inset of Fig. 7a) is used to describe the damping. The mass-spring-damper system is used to model the damping behavior of coalescing liquid marbles [52]. Since the viscosity of the droplet phase influences the damping of the oscillation [53], water is used as the only liquid phase of marbles encapsulated by different sizes of particles. Bare water and glycerol droplets are used as reference experiments for inertial-dominant coalescence and viscous-dominant coalescence (Video S6 and S7, respectively).

Our experiments reveal that different regimes of coalescence correspond to different damping scenarios. For the total coalescence case, the resulting marble oscillates before being finally stabilized (Video S8). This behavior is similar to the dynamics observed with bare water droplets but different from the non-oscillating glycerol droplet coalescence (⬡). The water droplet–droplet (⬡) and marble-marble coalescence (○) have comparable periods of oscillation of $t = 19.17$ ms and $t = 19.45$ ms, respectively, as shown in Fig. 7a. The oscillations are fitted using a least squares regression method for the data points after W_x reaches the first trough [54]. The oscillations are described by the equation $W_x = -Ae^{-\gamma t}\cos\omega_d t + B$, where A is the initial amplitude, γ is the damping factor directly related to the decay rate of the oscillations, ω_d is the damped natural frequency, and B is the width of the arrested marble [52]. This equation also applies to the case of arrested puddle coalescence (1 μm PTFE particle-coated marble-marble coalescence (□), Video S9) in Fig. 7b. The 1 μm PTFE particle-coated marbles coalesce in the puddle regime, but they display a transitional behavior with fast decaying oscillation. In this figure, the symbols represent the measurements, and the lines represent the best fits. The damping ratio $\zeta = \gamma/\sqrt{\omega_d^2 + \gamma^2}$ describes how the coalescence driven by the surface tension is stabilized by an impeding force. This impedance force can be the viscous force for the coalescence of high-viscosity droplets or the particle jamming for the coalescence of liquid marbles. The damping ratio ζ can vary from undamped ($\zeta = 0$), under-damped ($\zeta < 1$), critically damped ($\zeta = 1$), or overdamped (ζ greater than 1), when the impeding force becoming more pronounced [52]. For the total coalescence case, shown in Fig. 7a, the damping ratio ζ is smaller than 1, indicating that the total coalescence regime corresponds to the under-damped scenario.

For the arrested coalescence case shown in Fig. 7b, two liquid marbles coated with graphene nanoplates (□) (representative of arrested puddle coalescence, Video S10) and 6 μm silicone resin particles (△) (representative of arrested saddle coalescence, Video S11) do not exhibit any evident oscillations. The timescale before reaching arrested stabilized state is only a few tens of milliseconds, much smaller than our observation in the case of total coalescence and reveals a more damped behavior shown in the inset of Fig. 7b. A critically damped model, where the damping ratio ζ equals unity, is applied to the arrested coalescence dynamics (see details in Table S5, Supplementary Information). The corresponding non-oscillating solution is given by $W_x = (C + Dt)e^{-\gamma t} + E$, where C and D are two fitting constants, and E is the stabilized width. However, the dynamics of the marble-marble coalescence when one is stabilized by silica nanoparticles always follow an under-damped model (Fig. 7c). The damped natural frequency ω_d, the damping factor γ and the damping ratio ζ of the systems in Fig. 7a–c are extracted and listed in Table 1. These parameters reflect the differences between the coalescence regimes.

For the marble-marble coalescence reported in Fig. 7a and b, the different coalescence regimes reflect completely distinct long-time dynamics. For the total coalescence shown in Fig. 7a, while the coa-

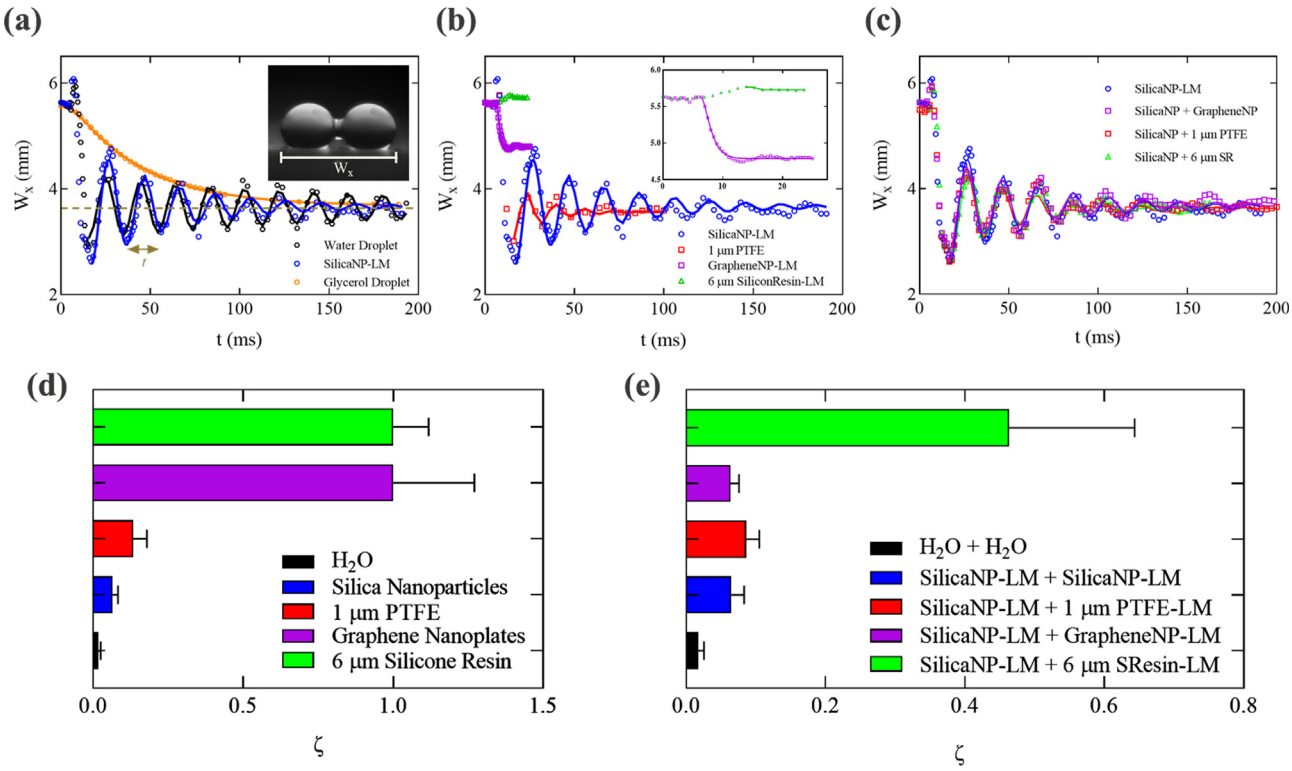

Fig. 7. Comparison of the coalescence dynamics of (a) liquid marbles coated with silica nanoparticles (○), bare glycerol droplets (⬡), and bare water droplets (⬡), (b) liquid marbles coated with silica nanoparticles (○), 1 μm PTFE particles (□), graphene nanoplates (□) and silicone resin microparticles (△), and (c) one liquid marble coated with silica nanoparticles while the other marble is coated with either silica nanoparticles (○), 1 μm PTFE particles (□), graphene nanoplates (□) or silicone resin microparticles (△). The hollow symbols represent the experimental measurements, and the solid lines represent the fitting curves. The damping ratios of the cases in (b) are shown in (d) and the ones in (c) are shown in (e), where the value of water droplets (control experiment) is added to both figures.

Table 1
Damped natural frequency, damping factor, and damping ratio of bare droplet–droplet coalescence and marble-marble coalescence of liquid marbles coated with various types of particle. 95% confidence interval is given from curve fitting.

	ω_d (kHz)	γ (ms^{-1})	ζ
Water droplet + Water droplet	0.324 ± 0.017	0.006 ± 0.003	0.017 ± 0.008
Glycerol droplet + Glycerol droplet	(undefined)	0.110 ± 0.010	1.560 ± 0.027
Silica nanoparticles + Silica nanoparticles	0.318 ± 0.004	0.021 ± 0.006	0.065 ± 0.018
1 μm PTFE particles + 1 μm PTFE particles	0.395 ± 0.013	0.053 ± 0.017	0.134 ± 0.046
Graphene nanoplates + Graphene nanoplates	0	0.944 ± 0.128	1.000 ± 0.271
6 μm Silicone resin + 6 μm Silicone resin	0	5.476 ± 0.325	1.000 ± 0.119
Silica nanoparticles + 1 μm PTFE particles	0.322 ± 0.004	0.028 ± 0.006	0.086 ± 0.019
Silica nanoparticles + Graphene nanoplates	0.312 ± 0.003	0.020 ± 0.004	0.064 ± 0.012
Silica nanoparticles + 6 μm Silicone resin	0.280 ± 0.003	0.170 ± 0.054	0.463 ± 0.180

lescence of liquid marbles coated by silica nanoparticles shows a similar natural frequency as that of bare water droplets, the introduction of silica nanoparticles increases the damping ratio ζ by a factor 4, from 0.017 to 0.065. The damping ratio of marble-marble coalescence keeps increasing for marbles stabilized with larger particles, increasing to 0.134 for 1 μm PTFE particles (Fig. 7b and d). For arrested coalescence, the value of the damping ratio is $\zeta = 1$, and the coalescence process is stopped without any subsequent oscillation. While having the same damping ratio ζ, a different damping factor γ is found to correspond to different degrees of arrested coalescence. For liquid marbles coated with 6 μm particles, the stabilized morphology corresponds to the arrested saddle coalescence regime, and the corresponding damping factor γ is 5.476, more than five-fold larger than that of marbles coated with graphene nanoplates corresponding to the arrested puddle coalescence regime. This observation indicates that arrested saddle coalescence has a higher decay rate of the oscillations than the arrested puddle coalescence. It also suggests that, for both arrested puddle and saddle coalescences where the damping ratio is unity, the numerical value of the damping factor γ directly reflects that the marbles in the saddle regime stabilize faster than in the puddle case.

The results for the marble-marble coalescence, where one marble LM_1 is coated with silica nanoparticles and the other marble LM_2 is coated with particles of other sizes, are summarized in Fig. 7c. Combined with the results presented in Fig. 7a, all cases demonstrate a total coalescence behavior as the Gaussian curvature of the stabilized droplets is around 1.9 for each case. This result suggests that for marble-marble coalescence, only one marble stabilized with large particles may not result in arrested structures. The experimental results show that particle jamming and arrested coalescence only occur when both marbles are stabilized with large particles. The coating particles show a limited influence on the damped natural frequency ω_d of the system, which varies by at most 12%. When the size of the stabilizing particles of LM_2 increases, an increment in the damping ratio ζ is observed. All

damping ratios for marble-marble coalescences are larger than that of bare water droplet–droplet coalescence, which is the smallest among all cases in Table 1 ($\zeta = 0.017$). Furthermore, in bare droplet–droplet coalescences, when the viscosity of the liquid phase is increased by replacing water with glycerol, the damping ratio ζ increases from 0.017 to 1.563. This increase indicates a transition from under-damped oscillation through critical damping to reach an overdamped behavior. By keeping water as the droplet phase, the damping ratio ζ increases from 0.065 to 0.463 as the size of the coating particles on LM_2 increases from hundreds of nanometers to 6 μm while that on LM_1 is kept at around hundreds of nanometers, as shown in Fig. 7e. The effect of larger particles can be reflected in a larger damping ratio, which shows that the oscillation would decay to reach stabilization at a faster rate.

The comparison of the coalescence of marble-marble and glycerol droplets shows that adding coating particles to the marbles leads to a similar effect as increasing the droplet viscosity. This can be reflected from the increased damping ratio above the baseline of water droplets' coalescence. Furthermore, the larger the coating particles are, the closer the damping ratio is to the viscous-dominant coalescence case, indicating an increase in the impeding force (Table 1). This further demonstrates the viscous-like behaviors during the coalescence of liquid drops when large particles armor the interface. For the arrested coalescence to occur, a large damping ratio is required and can be achieved by increasing the size of the particles that coat the liquid marble.

4. Conclusions

In this study, we characterized the influence of the size of the coating particles on the electrocoalescence dynamics of liquid marbles and the resulted arrested morphology. As shown in previous studies [31,55], the electrocoalescence of liquid marbles can be triggered by applying a sufficient voltage. We performed experiments by coating droplets with particles ranging from ~100 nm to ~100 μm. Our experiments revealed four distinct regimes characterized by the Gaussian curvature at the neck connecting the two coalesced liquid marbles: Total coalescence, arrested puddle coalescence, arrested saddle coalescence, and non-coalescence. The ability to generate non-spherical liquid marbles is due to the imbalance of the Laplace pressure within arrested structures, which is offset by the elastic modulus of the jammed particle layer, similar to other particle-laden systems [16,21].

Using high-speed imaging, we found the coalescence of liquid marbles always starts at a similar position - the center of the contact zone - independent of the size of coating particles. However, the subsequent coalescence behavior and the resulting morphology are determined by the size of the coating particles. Whereas the coalescence of liquid marbles has been widely studied, the role of the particle size on the coalescence dynamics and the resulting morphology of the final liquid marble remains elusive. In this study, we demonstrated that small particles show a negligible resistance to the coalescence of encapsulated water droplets while large particles lead to a viscous coalescence of the liquid marbles, indicated by the initially slow growth of the liquid bridge [9,29] and the subsequent heavily damped oscillation. Our work extends the understanding that the size of the coating particles can govern the shape of the resulting liquid marbles *via* distinct coalescence dynamics and provides guidelines for formulating morphologies of marble-based products and micro-reactors. In addition to the particle size, the degree of arrest is also expected to be related to how the particles modify the interfacial properties, which should be thoroughly investigated in future works. The results obtained in this study might further be extended to other particle-armored droplet systems, such as Pickering emulsions for which the dynamics is crucial in related biomedical applications, catalytic facilitation, and material synthesis.

CRediT authorship contribution statement

Yage Zhang: Conceptualization, Investigation, Formal analysis, Writing – review & editing. **Chentianyi Yang:** Investigation, Formal analysis, Writing – review & editing. **Shuai Yuan:** Investigation. **Xiaoxue Yao:** Writing – review & editing. **Youchuang Chao:** Writing – review & editing. **Yang Cao:** Visualization. **Qingchun Song:** Writing – review & editing. **Alban Sauret:** Writing – review & editing. **Bernard P. Binks:** Writing – review & editing. **Ho Cheung Shum:** Conceptualization, Writing – review & editing, Supervision.

Declaration of Competing Interest

The authors declare that they have no known competing financial interests or personal relationships that could have appeared to influence the work reported in this paper.

Acknowledgements

The authors would like to thank Prof. Huisheng Zhang, Dr. Zhou Liu, Dr. Tiantian Kong, Dr. Yuan Liu, and Dr. Qingchuan Li for helpful discussions on this work. This research was supported by the General Research Fund [grant numbers 17329516, 17304017] from the Research Grants Council of Hong Kong; the Excellent Young Scientists Fund (Hong Kong and Macau) [grant number 21922816] from the National Natural Science Foundation of China (NSFC); and the Sichuan Science and Technology Program [grant number 2018JZ0026].

Appendix A. Supplementary material

Supplementary data to this article can be found online at https://doi.org/10.1016/j.jcis.2021.09.187.

References

[1] E. Villermaux, Fragmentation versus cohesion, J. Fluid Mech. 898 (2020).
[2] Á. Moreno Soto, T. Maddalena, A. Fraters, D. van der Meer, D. Lohse, Coalescence of diffusively growing gas bubbles, J. Fluid Mech. 846 (2018) 143–165.
[3] M. Ruffert, H.T. Janka, W. Keil, G. Schaefer, Coalescing neutron stars as gamma ray bursters?, Astrophy Space Sci. 231 (1995) 423–426.
[4] R. Skibba, Fleeting phase of planet formation discovered, https://www.nature.com/news/fleeting-phase-of-planet-formation-discovered-1.22039.
[5] C. Andrieu, D.A. Beysens, V.S. Nikolayev, Y. Pomeau, Coalescence of sessile drops, J. Fluid Mech. 453 (2002) 427–438.
[6] N. Kapur, P.H. Gaskell, Morphology and dynamics of droplet coalescence on a surface, Phys. Rev. E 75 (2007) 056315.
[7] D.G.A.L. Aarts, H.N.W. Lekkerkerker, H. Guo, G.H. Wegdam, D. Bonn, Hydrodynamics of droplet coalescence, Phys. Rev. Lett. 95 (2005) 164503.
[8] B. Yuan, Z. He, W. Fang, X. Bao, J. Liu, Liquid metal spring: oscillating coalescence and ejection of contacting liquid metal droplets, Sci. Bull. 60 (2015) 648–653.
[9] A. Menchaca-Rocha, A. Martinez-Davalos, R. Nunez, S. Popinet, S. Zaleski, Coalescence of liquid drops by surface tension, Phys. Rev. E 63 (2001) 046309.
[10] J. Seemann, E. Jokitalo, M. Pypaert, G. Warren, Matrix proteins can generate the higher order architecture of the Golgi apparatus, Nature 407 (6807) (2000) 1022–1026.
[11] P. Dahiya, M. Caggioni, P.T. Spicer, Arrested coalescence of viscoelastic droplets: polydisperse doublets, Phil. Trans. R. Soc. A 374 (2016) 20150132.
[12] D. Rousseau, Fat crystals and emulsion stability - a review, Food Res. Int. 33 (1) (2000) 3–14.
[13] F. Thivilliers-Arvis, E. Laurichesse, V. Schmitt, F. Leal-Calderon, Shear-induced instabilities in oil-in-water emulsions comprising partially crystallized droplets, Langmuir 26 (22) (2010) 16782–16790.
[14] A.R. Studart, H.C. Shum, D.A. Weitz, Arrested coalescence of particle-coated droplets into nonspherical supracolloidal structures, J. Phys. Chem. B 113 (2009) 3914.

[15] M. Cui, T. Emrick, T.P. Russell, Stabilizing liquid drops in nonequilibrium shapes by the interfacial jamming of nanoparticles, Science 342 (6157) (2013) 460–463.
[16] A.B. Subramaniam, M. Abkarian, L. Mahadevan, H.A. Stone, Colloid science: non-spherical bubbles, Nature 438 (2005) 930.
[17] M. Abkarian, A.B. Subramaniam, S.H. Kim, R.J. Larsen, H.A. Stone, Dissolution arrest and stability of particle-covered bubbles, Phys. Rev. Lett. 99 (2007) 188301.
[18] K. Stratford, R. Adhikari, I. Pagonabarraga, J.C. Desplat, M.E. Cates, Colloidal jamming at interfaces: a route to fluid-bicontinuous gels, Science 309 (2005) 2198–2201.
[19] E.M. Herzig, K.A. White, A.B. Schofield, W.C.K. Poon, P.S. Clegg, Bicontinuous emulsions stabilized solely by colloidal particles, Nat. Mater. 6 (12) (2007) 966–971.
[20] B.P. Binks (Ed.), Modern Aspects of Emulsion Science, The RSC, Cambridge, 1998.
[21] A.B. Pawar, M. Caggioni, R. Ergun, R.W. Hartel, P.T. Spicer, Arrested coalescence in Pickering emulsions, Soft Matter 7 (17) (2011) 7710–7716.
[22] Z. Xie, C.J. Burke, B. Mbanga, P.T. Spicer, T.J. Atherton, Geometry and kinetics determine the microstructure in arrested coalescence of Pickering emulsion droplets, Soft Matter 15 (46) (2019) 9587–9596.
[23] D. Chen, E. Amstad, C.-X. Zhao, L. Cai, J. Fan, Q. Chen, M. Hai, S. Koehler, H. Zhang, F. Liang, Z. Yang, D.A. Weitz, Biocompatible amphiphilic hydrogel-solid dimer particles as colloidal surfactants, ACS Nano 11 (12) (2017) 11978–11985.
[24] M. Rayner, A. Timgren, M. Sjoo, P. Dejmek, Quinoa starch granules: a candidate for stabilising food-grade Pickering emulsions, J. Sci. Food Agric. 92 (2012) 1841–1847.
[25] Y. Timounay, O. Pitois, F. Rouyer, Gas marbles: much stronger than liquid marbles, Phys. Rev. Lett. 118 (2017) 228001.
[26] N. Taccoen, F. Lequeux, D.Z. Gunes, C.N. Baroud, Probing the mechanical strength of an armored bubble and its implication to particle-stabilized foams, Phys. Rev. X 6 (2016) 011010.
[27] P. Aussillous, D. Quéré, Liquid marbles, Nature 411 (6840) (2001) 924–927.
[28] P. Aussillous, D. Quéré, Properties of liquid marbles, Proc. Roy. Soc. A 462 (2067) (2006) 973–999.
[29] Jens Eggers, John R. Lister, Howard A. Stone, Coalescence of liquid drops, J. Fluid Mech. 401 (1999) 293–310.
[30] F. Sarvi, K. Jain, T. Arbatan, P.J. Verma, K. Hourigan, M.C. Thompson, W. Shen, P. P.Y. Chan, Cardiogenesis of embryonic stem cells with liquid marble micro-bioreactor, Adv. Healthc. Mater. 4 (1) (2015) 77–86.
[31] Y. Zhang, X. Fu, W. Guo, Y.i. Deng, B.P. Binks, H.C. Shum, Electrocoalescence of liquid marbles driven by embedded electrodes for triggering bioreactions, Lab Chip 19 (20) (2019) 3526–3534.
[32] X. Han, H.K. Lee, Y.H. Lee, W. Hao, Y. Liu, I.Y. Phang, S. Li, X.Y. Ling, Identifying enclosed chemical reaction and dynamics at the molecular level using shell-isolated miniaturized plasmonic liquid marble, J. Phys. Chem. Lett. 7 (8) (2016) 1501–1506.
[33] F. Geyer, Y. Asaumi, D. Vollmer, H.-J. Butt, Y. Nakamura, S. Fujii, Polyhedral liquid marbles, Adv. Funct. Mater. 29 (2019) 1808826.
[34] Y. Chu, Z. Wang, Q. Pan, Constructing robust liquid marbles for miniaturized synthesis of graphene/Ag nanocomposite, ACS Appl. Mater. Interfaces 6 (11) (2014) 8378–8386.
[35] B.T. Lobel, P.M. Ireland, L.M. Walsh, C.A. Thomas, G.B. Webber, E.J. Wanless, Electrostatic transfer of conductive particles for the formation of liquid marbles–Charge transfer behavior, J. Phys. Chem. C 124 (18) (2020) 9947–9957.
[36] E. Bormashenko, R. Pogreb, G. Whyman, A. Musin, Surface tension of liquid marbles, Colloids Surf. A Physicochem. Eng. Asp. 351 (1-3) (2009) 78–82.
[37] Y. Asaumi, M. Rey, K. Oyama, N. Vogel, T. Hirai, Y. Nakamura, S. Fujii, Effect of stabilizing particle size on the structure and properties of liquid marbles, Langmuir 36 (44) (2020) 13274–13284.
[38] T.Q. Liu, W. Sun, X.Y. Sun, H.R. Ai, Mechanism study of condensed drops jumping on super-hydrophobic surfaces, Colloids Surf. A Physicochem. Eng. Asp. 414 (2012) 366–374.
[39] J. Gregory, Approximate expressions for retarded van der waals interaction, J. Colloid Interface Sci. 83 (1) (1981) 138–145.
[40] D.F. Williams, J.C. Berg, The aggregation of colloidal particles at the air-water interface, J. Colloid Interface Sci. 152 (1) (1992) 218–229.
[41] C. Planchette, A.L. Biance, E. Lorenceau, Transition of liquid marble impacts onto solid surfaces, Europhys. Lett. 97 (2012) 14003.
[42] X. Li, R. Wang, H. Shi, B. Song, Effective surface tension of liquid marbles using controllable nanoparticle monolayers, Appl. Phys. Lett. 113 (2018) 101602.
[43] N. Eshtiaghi, J.S. Liu, W. Shen, K.P. Hapgood, Liquid marble formation: spreading coefficients or kinetic energy?, Powder Technol 196 (2009) 126–132.
[44] B.P. Binks, T. Horozov, Colloidal Particles at Liquid Interfaces, Cambridge University Press, 2006.
[45] M.I. Newton, D.L. Herbertson, S.J. Elliott, N.J. Shirtcliffe, G. McHale, Electrowetting of liquid marbles, J. Phys. D 40 (1) (2007) 20–24.
[46] A.N. Pressley, Elementary Differential Geometry, Springer-Verlag, London, 2010.
[47] P. Singha, N.K. Nguyen, K.R. Sreejith, H. An, N.T. Nguyen, C.H. Ooi, Effect of core liquid surface tension on the liquid marble shell, Adv. Mater. Interfaces 8 (2021) 2001591.
[48] X. Li, Y. Wang, J. Huang, Y. Yao, R. Wang, X. Geng, D. Zang, Monolayer nanoparticle-covered liquid marbles derived from a sol-gel coating, Appl. Phys. Lett. 111 (2017) 261604.
[49] D. Vella, P. Aussillous, L. Mahadevan, Elasticity of an interfacial particle raft, Europhys. Lett. 68 (2) (2004) 212–218.
[50] Z. Liu, Y. Zhang, T. Yang, Z. Wang, H.C. Shum, Compressed liquid marble ruptures at edge, Appl. Phys. Lett. 114 (2019) 243701.
[51] R.T. Eiswirth, H.J. Bart, A.A. Ganguli, E.Y. Kenig, Experimental and numerical investigation of binary coalescence: liquid bridge building and internal flow fields, Phys. Fluids 24 (2012) 140–141.
[52] R.C. Hibbeler, Engineering Mechanics: Statics & Dynamics, Pearson Education, Delhi, 2007.
[53] J. Zheng, H. Shi, G. Chen, Y. Huang, H. Wei, S. Wang, W. Wen, Relaxation of liquid bridge after droplets coalescence, AIP Adv. 6 (2016) 115115.
[54] K.P. Chong Edwin, H.Z. Stanislaw, An Introduction to Optimization, Wiley, New York, 2004.
[55] X. Fu, Y. Zhang, H. Yuan, B.P. Binks, H.C. Shum, Controlled actuation of liquid marbles on a dielectric, ACS Appl. Mater. Interfaces 10 (41) (2018) 34822–34827.